Analytic diffraction analysis of a 32-m telescope with hexagonal segments for high-contrast imaging

Erin Sabatke, James Burge, and Derek Sabatke

Large segmented telescopes cannot be modeled accurately with fast-Fourier-transform techniques since small features such as gaps between the segments will be inadequately sampled. An analytic Fourier-transform method can be used to model any pupil configuration with straight edges, including tolerance analysis and some types of apodization. We analytically investigated a 32-m segmented primary with 18 hexagonal segments for high-contrast imaging. There are significant regions in the image in which extrasolar planets could be detected. However, the hexagonal profile of the pupil was not as useful as expected. The gaps between the segments, the secondary obscuration, and the secondary spiders must be as small as possible and their edges must be apodized. Apodizing the edges of the individual segments reduced the useful regions in the image since the gaps appeared to be wider.

OCIS codes: 350.1260, 110.6770.

1. Introduction

Ground-based telescopes with single primaries 30 m in diameter have been proposed. Such a diameter may allow planet imaging from the ground if images of high contrast can be achieved over regions large enough for planet detection.[1,2] Most of the proposed primary configurations use segmented mirrors.[3,4] For a proposed primary configuration consisting of segments with gaps between them, diffractive modeling is needed to reveal the image and how that image is affected by pupil configuration; gap width; apodization; and mispositioning, piston, and tilt errors on the individual segments.

Fast-Fourier-transform (FFT) techniques are usually used to calculate the image from a complex pupil.[5] For 30-m telescopes, however, the gaps between the segments are often small compared to the segment diameters. For example, one proposed configuration uses 8-m hexagonal segments in a 32-m primary with 30-mm gaps between the segments.[3] Use of FFT calculations to see the effects of the gaps on the system's image would require at least ten pixels across a gap, which leads to an unmanageable array size of over $10{,}000^2$.

The solution can often be calculated analytically instead. The Fourier transform of virtually any pupil function with only straight edges can be calculated by geometric integration and the properties of the Fourier transform. In this paper we explain this method and how it is used to explore the behavior of a 30-m primary with hexagonal segments.

2. Useful Properties of the Fourier Transform

The goal is to calculate the intensity in the image plane $I(x, y)$ due to a complex pupil function. Fraunhofer diffraction theory[6] states that the image plane intensity is related to the complex square of the Fourier transform of the pupil function:

$$I(x, y) = \left(\frac{1}{\lambda f}\right)^2 \left\| \left\{ \int\int f(x, y) \exp[i2\pi\phi(x, y)/\lambda] \times \exp[i2\pi(\xi y + \eta x)]\delta x \delta y \right\}_{\xi \to y/\lambda f, \eta \to x/\lambda f} \right\|^2, \quad (1)$$

where $f(x, y)$ is the apodizing function across the pupil and $\phi(x, y)$ is any phase error that might be present in the pupil. The Fourier kernel is the term $\exp[i2\pi(\xi y + \eta x)]$. The integration is carried out over the area of the pupil, and it results in a function of the spatial-frequency coordinates ξ and η. These can be

The authors are with the Optical Sciences Center, University of Arizona, 1630 East University Boulevard, Tucson, Arizona 85721. E. Sabatke's e-mail address is esabatke@ball.com.

Received 20 September 2004; revised manuscript received 25 October 2004; accepted 26 October 2004.

0003-6935/05/081360-06$15.00/0

converted to real space coordinates x and y by the transformations $\xi \rightarrow y/(\lambda f)$ and $n \rightarrow x/(\lambda f)$ where λ is the wavelength under consideration and f is the focal length of the telescope. Alternatively, ξ and η can be converted to angular coordinates on the sky by the transformations $\xi \rightarrow y/\lambda$ and $\eta \rightarrow x/\lambda$.

The Fourier-transform operation has several useful properties that will aid in the calculation of $I(x, y)$.[7] These are

- Linearity: The transform of a sum of two functions is the sum of their individual transforms. This is a restatement of Babinet's principle.
- Shift: The Fourier transform of a shifted function is the transform of the unshifted function multiplied by a linear phase factor.
- Rotation: The Fourier transform of a rotated function is the rotated Fourier transform of the unrotated function.

Under the linearity property, Eq. (1) becomes a summation of k pieces within the pupil that do not overlap and each integration is carried out over only the area of the kth piece:

$$I(x, y) = \left(\frac{1}{\lambda f}\right)^2 \left\| \left\{ \sum_k \int\int f_k(x, y) \exp[i2\pi\phi_k(x, y)/\lambda] \times \exp[i2\pi(\xi y + \eta x)]\delta x \delta y \right\}_{\xi \rightarrow y/\lambda f,\ \eta \rightarrow x/\lambda f} \right\|^2, \quad (2)$$

The properties of shift and rotation allow the transform of each piece k to be calculated in any convenient coordinate system. The resulting Fourier transform can be adjusted for the shift and rotation required to return the kth piece to its proper position in the pupil. Let $f(x, y)$ be a known pupil function and $g(\xi, \eta)$ be its Fourier transform, as shown in Eq. (3). The transform of the same function shifted by (x_0, y_0) and rotated by θ is given in Eq. (4):

$$\mathcal{F}[f(x, y)] = g(\xi, \eta), \quad (3)$$

$$\mathcal{F}\{f(x - x_0, y - y_0, \theta)\} = \exp[i2\pi(x_0\eta + y_0\xi)]g(\xi \cos\theta + \eta \sin\theta, -\xi \sin\theta + \eta \cos\theta), \quad (4)$$

where $\mathcal{F}$ is the Fourier-transform operation and θ is positive for a clockwise rotation.

These three Fourier-transform properties combined show that the Fourier transform of any pupil can be calculated if the pupil is the sum of smaller pieces that do not overlap and whose Fourier transforms are known. The problem in Eq. (1) is reduced to calculating $\int\int f_k(x, y)\exp[i2\pi\phi_k(x, y)/\lambda]\exp[i2\pi(\xi y + \eta x)]\delta x \delta y$ in any convenient coordinate system for each of the pieces in the pupil.

3. Analytic Fourier Transform of a Hexagon and Related Systems

Any pupil with straight edges can be broken up into smaller pieces whose Fourier transform is easy to calculate. As an example, consider a regular hexagon. The hexagon can be seen as the sum of two trapezoids as shown in Fig. 1. Assume there is no apodization so that $f(x, y) = 1$, and also assume that there is no phase error so that $\phi(x, y) = 0$. Let D be the flat-to-flat width of the hexagon.

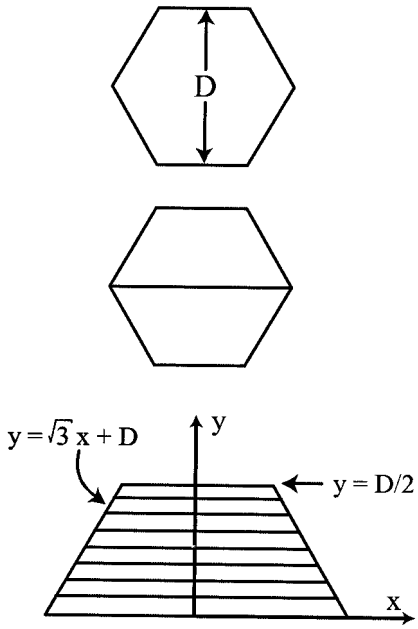

Fig. 1. Regular hexagon is the sum of two trapezoids, and each trapezoid is the sum of strips whose length depends on the height of the strip in the trapezoid.

To calculate the analytic transform, consider the upper trapezoid to be the sum of an infinite number of horizontal strips, as shown in Fig. 1. The end points of the strips are given by the sides of the trapezoid: $x = (y - D)/\sqrt{3}$ and $x = (y - D)/(-\sqrt{3})$. The sum of the strips from $y = 0$ to $y = D/2$ gives the complete Fourier transform of the trapezoid g:

$$\begin{aligned} g(\xi, \eta) &= \int_0^{D/2} \left\{ \int_{(y-D)/\sqrt{3}}^{(y-D)/(-\sqrt{3})} \exp[i2\pi(\xi y + \eta x)]\delta x \right\} \delta y \\ &= \frac{\exp\left[-i\pi D\left(\frac{2\eta}{\sqrt{3}} + \xi\right)\right]}{4\pi^2(\eta^3 - 3\eta\xi^2)} \Bigg((\sqrt{3}\eta - 3\xi) \\ &\quad \times \left\{ \exp(i\pi D\sqrt{3}\eta) - \exp\left[i\pi D\left(\frac{4}{\sqrt{3}}\eta + \xi\right)\right] \right\} \\ &\quad + (\sqrt{3}\eta + 3\xi)\left[\exp(i\pi D\eta/\sqrt{3}) - \exp(i\pi D\xi)\right] \Bigg). \end{aligned} \quad (5)$$

The transform of the entire hexagon must be the sum of the two trapezoids, one of which is rotated about the origin by 180°:

$$\mathrm{hex}(\xi, \eta) = g(\xi, \eta) + g(-\xi, \eta), \quad (6)$$

and the intensity in the image plane will be

$$\left(\frac{1}{\lambda f}\right)^2 \left\| \mathrm{hex}\left(\frac{y}{\lambda f}, \frac{x}{\lambda f}\right)\right\|^2. \tag{7}$$

The image from the hexagonal pupil is plotted in Fig. 2.

The FFT technique is now useful as a check that the analytic answer is correct. The analytic Fourier transform of the hexagon f can be sampled rather coarsely and an inverse FFT applied. The complex square of the result gives the original pupil intensity, as shown in Fig. 2.

We can now easily apply the properties of the Fourier transform discussed above to calculate the Fourier transform of more complicated hexagonal-based pupils without carrying out further integrations. Table 1 lists some useful cases. The cases showing position, piston, and tilt errors can be used to examine the tolerances of the primary mirror segments. The tilt terms indicate a phase error across the hexagonal segment of $\exp[i2\pi(\alpha y + \beta x)/\lambda]$.

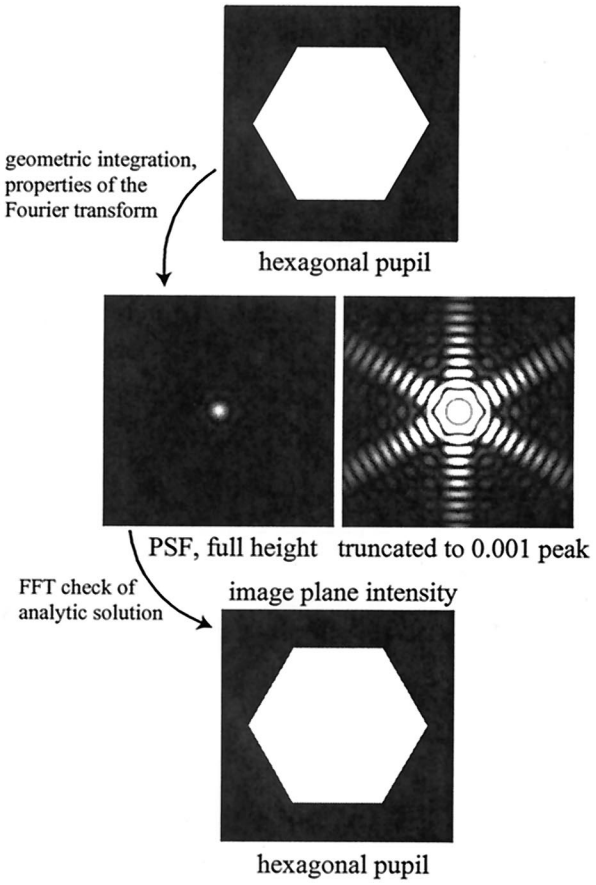

Fig. 2. Image intensity from a hexagonal pupil can be calculated analytically. As a check, a FFT can then be applied to the image amplitude to recover the original pupil amplitude.

4. Apodization

The images from pupils with apodization can also be calculated analytically in some cases. Consider the apodized hexagon shown in Fig. 3. It contains just two shapes: a trapezoid with a constant amplitude of 1 and a smaller trapezoid with a cosine-squared profile.

Let the flat-to-flat width of the hexagon again be D and the width of each apodizing strip be ε. The Fourier transforms of sections A and B are

$$\mathrm{A}(\xi, \eta) = \int_0^{\frac{(D-2\varepsilon)}{2}} \int_{\frac{y-(D-2\varepsilon)}{\sqrt{3}}}^{\frac{y-(D-2\varepsilon)}{-\sqrt{3}}} \exp[i2\pi(\xi y + \eta x)]\delta x \delta y, \tag{8}$$

$$\mathrm{B}(\xi, \eta) = \int_0^{\varepsilon} \int_{\frac{(y-D/2)}{\sqrt{3}}}^{\frac{(y-D/2)}{-\sqrt{3}}} \left[\cos\frac{\pi(\varepsilon - y)}{2\varepsilon}\right]^2 \times \exp[i2\pi(\xi y + \eta x)]\delta x \delta y, \tag{9}$$

Table 1. Useful Hexagonal Fourier Transforms

Pupil Shape	Fourier Transform of the Pupil
Trapezoid	$g(\xi, \eta) = \int_0^{D/2} \{\int_{(y-D)/\sqrt{3}}^{(y-D)/-\sqrt{3}} \exp[i2\pi(\xi y + \eta x)]\delta x\}\delta y$
Regular hexagon	$\mathrm{hex}(\xi, \eta) = g(\xi, \eta) + g(-\xi, \eta)$
Two hexagons, flat sides together, gap of δ between them	$h_1(\xi, \eta) = \exp[i\pi(D + \delta)\eta]\mathrm{hex}\left(\xi\cos\frac{\pi}{6} + \eta\sin\frac{\pi}{6}, -\xi\sin\frac{\pi}{6} + \eta\cos\frac{\pi}{6}\right)$, $h_2(\xi, \eta) = \exp[-i\pi(D + \delta)\eta]\mathrm{hex}\left(\xi\cos\frac{\pi}{6} + \eta\sin\frac{\pi}{6}, -\xi\sin\frac{\pi}{6} + \eta\cos\frac{\pi}{6}\right)$, $h_{\mathrm{total}}(\xi, \eta) = h_1(\xi, \eta) + h_2(\xi, \eta)$
Two hexagons with position errors $(\delta x_1, \delta y_1, \delta x_2, \delta y_2)$	$\exp[i2\pi(\delta x_1\eta + \delta y_1\xi)]h_1(\xi, \eta) + \exp[i2\pi(\delta x_2\eta + \delta y_2\xi)]h_2(\xi, \eta)$
Two hexagons with piston errors p_1 and p_2 in units of distance	$\exp(i2\pi p_1/\lambda)h_1(\xi, \eta) + \exp(i2\pi p_2/\lambda)h_2(\xi, \eta)$
Two hexagons with tilt errors $(\alpha_1, \beta_1, \alpha_2, \beta_2)$ in radians	$h_1\left(\xi - \frac{\alpha_1}{\lambda}, \eta - \frac{\beta_1}{\lambda}\right) + h_2\left(\xi - \frac{\alpha_2}{\lambda}, \eta - \frac{\beta_2}{\lambda}\right)$

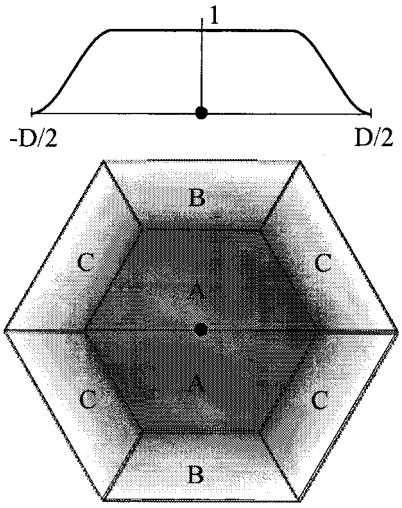

Fig. 3. Apodized hexagon and its cross section, which falls off as $\cos^2$.

The regions C are shifted and rotated versions of B:

$$\mathrm{C}(\xi,\ \eta) = \exp\left[-i2\pi\left(\frac{D}{4}\,\xi + \frac{\sqrt{3}D}{4}\,\eta\right)\mathrm{B}\left(\xi\cos\frac{2\pi}{3} - \eta\sin\frac{2\pi}{3},\ \xi\sin\frac{2\pi}{3} + \eta\cos\frac{2\pi}{3}\right)\right]. \quad (10)$$

The Fourier transform of the entire segment G is then a sum of these functions with the proper shifts and rotations:

$$\begin{aligned}\mathrm{G}(\xi,\ \eta) = {} & \mathrm{A}(\xi,\ \eta) + \mathrm{A}(-\xi,\ \eta) + \exp(i\pi D\xi)\mathrm{B}(\xi,\ \eta) \\ & + \exp(-i\pi D\xi)\mathrm{B}(-\xi,\ \eta) + \mathrm{C}(\xi,\ \eta) \\ & + \mathrm{C}(-\xi,\ \eta) + \mathrm{C}(-\xi,\ -\eta) + \mathrm{C}(\xi,\ -\eta).\end{aligned} \quad (11)$$

5. Investigation of a 32-m Primary Mirror

The techniques above were used to investigate the performance of a hexagonal primary with a diameter of 32 m, as shown in Fig. 4. The hexagonal shape was chosen so that the majority of the diffracted light would lie in six arms in the diffracted image, leaving significant regions with low background available for planet imaging. The system investigated here has 18 hexagonal segments with inner diameters of 8 m. The gaps between the segments are ~ 30 mm. The secondary supports were taken to be 0.50 m in width, and the obscuration was assumed to be a hexagon with an 8-m flat-to-flat diameter.

Figure 4 shows the analytic point-spread function (PSF) of the hexagonal pupil. It was truncated to 1/1000 of its peak height so that sidelobe detail is visible. The pupil is also shown, which we reconstructed from the analytic PSF using FFT techniques.

Figure 5 shows the four types of pupil that were investigated: the perfect hexagonal pupil, the segmented pupil with secondary and spider obscura-

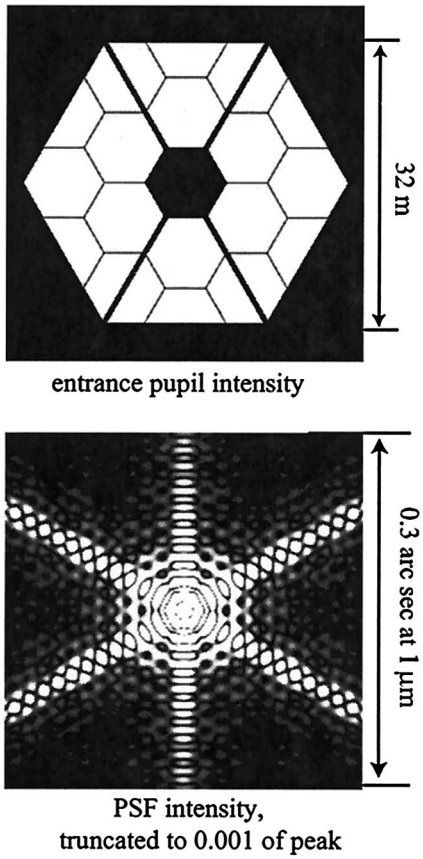

Fig. 4. Analytic PSF irradiance plot for a segmented hexagonal primary 32 m in diameter, with spider supports and secondary.

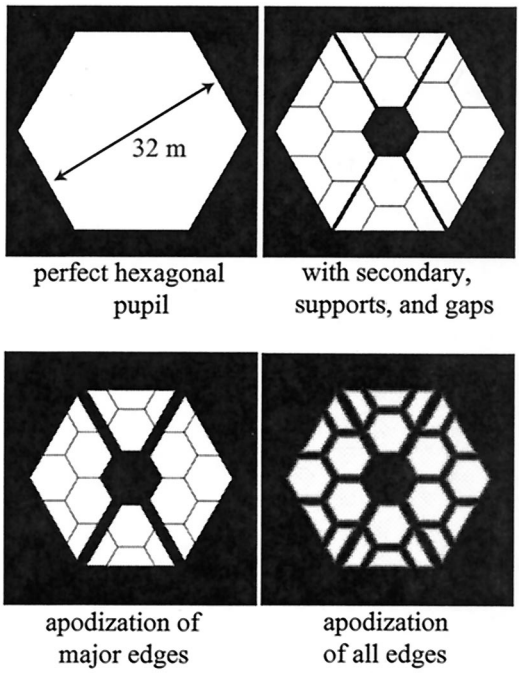

Fig. 5. System performance was evaluated with and without the secondary and supports, with varying gap widths, and with two styles of apodization.

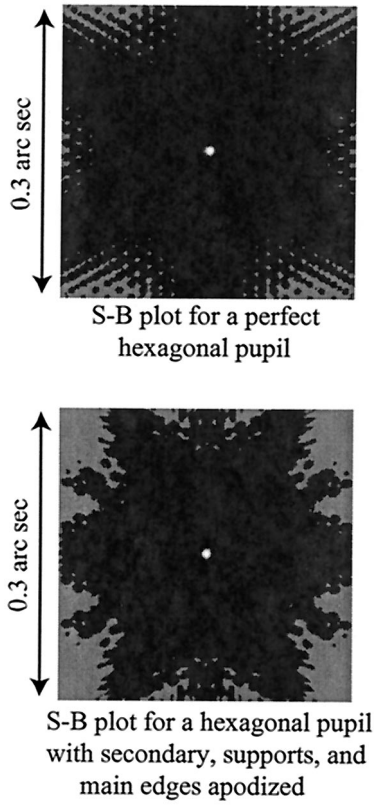

Fig. 6. Regions where planet detection is possible are shown in gray for a perfect hexagonal pupil and for a hexagonal pupil with secondary, supports, and the major edges apodized. The star's PSF is shown at the center. S–B, signal-to-background.

tions, the pupil with apodization of the outside edges and obscurations, and the pupil with every hard edge apodized. Widths of the gaps and apodization were varied for each case.

To evaluate the potential for finding planets with these pupil configurations, signal-to-background plots were created. Angel has shown that contrasts of 10^{-7} will be adequate for planet imaging, assuming an 8-h exposure time, a 30-m primary, a bandwidth of 0.85 ± 0.15 μm, and a specialized system.[8] The planet was assumed to have a circular PSF with the same width as the FWHM of the central peak of the star's PSF. A discrete convolution of the scaled planet signal with the star's PSF revealed the locations for which the signal-to-background value would be one or greater. An example of the resulting signal-to-background plots is shown in Fig. 6.

We could reduce the signal-to-background plots to a single number by summing over the area inside the star's twentieth Airy ring (at 0.3 arc sec) and scaling, giving the percentage of usable area for planet imaging. The wavelength used for the calculations was 1 μm. Polychromatic calculations with a 10% bandwidth showed no significant departures from the monochromatic results.

For a perfect hexagonal primary of 32 m, the usable area was 7.3%, but dropped to just 1% after we accounted for the secondary and supports. This suggests that constraining the pupil shape to hexagonal is not useful when realistic details such as secondaries and supports are accounted for. Adjusting the segments' gap widths for the unapodized pupil configuration had little effect on the system performance since it was dominated by the secondary and supports.

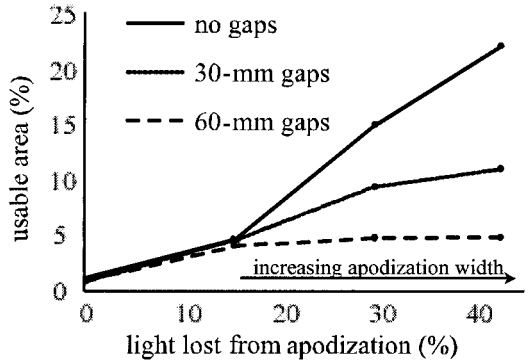

Fig. 7. Apodizing the main edges in the primary led to an improvement in the area usable for planet imaging, defined as regions where the signal-to-background ratio is greater than 1. The loss of performance due to the widening of the gaps is clearly visible.

Apodization of the pupil, secondary, and spider edges improved the performance but increased the significance of the gap widths, as shown in Fig. 7. With a 42.8% loss of light due to the apodization of the main edges, the usable area in the signal-to-background plot rose to 22% in the unrealistic case of no gaps. The signal-to-background plots for the system with and without the main edges apodized are shown in Fig. 6. Both plots include the effects of the obscuration and supports and have gap widths of zero.

With the major edges apodized, the system proved to be fairly sensitive to phase errors. For example, with the system apodized to 55.6% transmission, piston errors with an average of 0.01 waves led to a 17% reduction in usable area. Piston errors with an average of 0.05 waves led to a drastic 85% reduction in usable

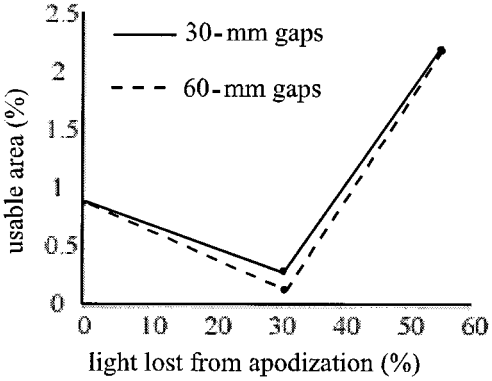

Fig. 8. Apodization of the individual segments initially leads to a loss in performance because the gaps between segments appear to be wider. Performance recovers somewhat as the apodization width increases.

area. Tilt and positional errors in the plane of the primary have not yet been investigated for this system.

Apodizing the edges of the individual segments initially causes the gaps to seem wider, reducing the performance. The performance is not improved by the gaps' apodization until this performance loss is overcome, which is at roughly 45% loss of light in the system investigated here (see Fig. 8).

6. Conclusions

For a hexagonal primary with an inner diameter of 32 m, there are significant regions for which planet imaging is possible. To achieve such regions, the gaps between the segments, secondary obscuration, and secondary spiders must be as small as possible. The major edges in the system must be apodized. For gaps of 30 mm and apodization that leads to a loss of 29.7% of the light, the usable area inside 0.3 arc sec is 9.3%. Without apodization, the usable area dropped to 0.9%.

Designing the system to have hexagonal symmetry did not prove to be as useful as expected. The diffraction pattern did have six arms, but the details of the secondary and the spider arms interfered with the production of the low background regions between the arms.

Apodizing all the edges in the system with the apodization function tested here led to no performance gains because the apodization initially caused the gaps to appear wider, decreasing the performance and canceling out the benefits of apodization.

This research was supported by California Institute of Technology and National Science Foundation grant AST-0138347.

References

1. R. Angel, "Ground-based imaging of extrasolar planets using adaptive optics," Nature (London) **368,** 203–207 (1994).
2. P. Nisenson and C. Papaliolios, "Detection of earth-like planets using apodized telescopes," Astrophys. J. **548,** L201–L205 (2001).
3. J. R. P. Angel, J. H. Burge, J. L. Codona, W. B. Davison, and B. Martin, "20- and 30-m telescope designs with potential for subsequent incorporation into a track-mounted pair (20/20 or 30/30)," in *Future Giant Telescopes*, J. R. P. Angel and R. Gilmozzi, eds., Proc. SPIE **4840,** 1223–1232 (2002).
4. J. E. Nelson, "Design concepts for the California Extremely Large Telescope (CELT)," in *Telescope Structures, Enclosures, Controls, Assembly/Integration/Validation, and Commissioning*, T. A. Sebring and T. Anderson, eds., Proc. SPIE **4004,** 282–289 (2000).
5. J. Hayes, "Fast Fourier transforms and their application," in *Applied Optics and Optical Engineering*, 11th ed. (Academic, San Diego, Calif., 1992), Vol. 2, Chap. 2, pp. 55–123.
6. J. W. Goodman, *Introduction to Fourier Optics*, 2nd ed. (McGraw-Hill, New York, 1996).
7. J. Gaskill, *Linear Systems, Fourier Transforms, and Optics* (Wiley, New York, 1978).
8. R. Angel, "Imaging planets from the ground," in *Scientific Frontiers in Research on Extrasolar Planets,* Vol. 294 of ASP Conference Series, S. Seager and D. Deming, eds. (Astronomical Society of the Pacific, San Francisco, Calif., 2003), pp. 543–555.